Fibers and Polymers 2016, Vol.17, No.12, 2006-2013
DOI 10.1007/s12221-016-6821-0

ISSN 1229-9197 (print version)
ISSN 1875-0052 (electronic version)

Characterization and Antibacterial Properties of Ag NPs Doped Nylon 6 Tree-like Nanofiber Membrane Prepared by One-step Electrospinning

Weimin Kang, Jingge Ju, Huihui Zhao, Zongjie Li, Xiaomin Ma, and Bowen Cheng[1]*

College of Textile, Tianjin Polytechnic University, Tianjin 300387, P.R. China
[1]*State Key Laboratory of Separation Membranes and Membrane Processes, Tianjin Polytechnic University, Tianjin 300387, P.R. China*

(Received August 12, 2016; Revised November 1, 2016; Accepted November 4, 2016)

Abstract: A hierarchically Ag/nylon 6 tree-like nanofiber membrane (Ag/PA6 TLNM) was fabricated by adding tetrabutylammonium chloride (TBAC) and silver nitrate ($AgNO_3$) into spinning solution via one-step electrospinning. TBAC presented in PA6/formic acid (HCOOH) spinning solution was able to cause the formation of a tree-like structure due to its space steric structure and the increasing of solution conductivity. Electrospinning solvent acted as a reducing agent for in situ conversion of $AgNO_3$ into silver nanoparticles (Ag NPs) during the solution preparation. SEM, TEM, FT-IR XPS and XRD confirmed that Ag NPs were doped in the prepared nanofiber membrane successfully and the mechanical properties, pore size distribution and hydrophilicity of the membranes were investigated. The results showed that the tree-like structure improved the mechanical properties and hydrophilicity of the membrane while ensuring high specific surface area and small pore size. And the Ag/PA6 TLNM showed superior antibacterial properties against both *E. coli* and *S. aureus* compared with common Ag/PA6 nanofiber membranes (Ag/PA6 NMs). All of the results show that the Ag/PA6 TLNM would have potential applications in water purification.

Keywords: Electrospinning, Tree-like, Nanofiber membrane, Ag NPs, Antibacterial

Introduction

In recent years, there has been an increasing concern on antibacterial products in application areas such as water purification, protection, wound dressing, etc [1-3]. Ag nanoparticles (Ag NPs), which could damage the membrane structure of bacteria [4], have no adversely affect to viable cells and do not easily provoke microbial resistance [5], have been widely used as additives of biomedical products, such as beads, gels, films and fibers, to enhance the antibacterial ability of the materials [6-8].

As a simple and effective technology, electrospinning has received great attentions to produce nanofiber membranes with outstanding properties, such as high specific surface area, high porosity and outstanding interconnected pore structure [9]. The combination of these advantages with the biocidal activity of Ag NPs resulted in superior and versatile antimicrobial materials [10-13]. PA6 is a widely used organic polymer, which exhibits low cost, strong chemical and thermal stability [14,15] and had been used in filtration, biomedicine and protection, etc [16,17]. Francis *et al.* [18] had fabricated a nylon-silver composite nanofiber membrane via electrospinning and ethylene glycol was used as a reducing agent for $AgNO_3$. Quan *et al.* [19] reported a novel and facile one-step approach to in situ synthesize silver nanoparticle-doped nylon 6 nanofibers by using the electrospinning solvent (formic acid) as a reducing agent and the electrospinning polymer as a stabilizing agent. The method was simple and energy-saving compared with the two-step process [20,21].

Recent years, micro-/nano combined hierarchically structure fibers had received considerable attentions. Bai *et al.* [22] fabricated a ZnO/Cu "corn-like" material via a facile low temperature hydrothermal and photo-deposition methods and the corn-like structure improved the photocatalytic activity and antibacterial capability of the materials through enlarging the specific surface area for mass transfer and providing more reaction sites. Ding *et al.* [23] fabricated a hierarchically spider-web like nanofiber membrane by adding inorganic salt into spinning solution via electrospinning and the novel nanofiber membrane contained common electrospun nanofibers (100-1000 nm) and spider web-like nanofibers (5-40 nm). The common nanofibers acted as supports for the spider web-like nano-nets while spider web-like nano-nets endowed the membrane high specific surface area and small pore size, resulting in excellent properties in filtration, tissue engineering, protective clothing and sensors [23-25]. Besides, Pant also fabricated a spider-web like PA6 nanofiber membrane by adding MPEG or TiO_2 into spinning solution and the membrane showed excellent mechanical properties, UV blocking and antibacterial properties [26,27]. Our team had fabricated a hierarchically PVDF tree-like nanofiber membrane by adding certain amount of TBAC into PVDF/DMF/acetone solution via one-step electrospinning and the tree-like nanofiber membrane was composed of trunk fibers and branch fibers, among them, the thick trunk fibers acted as a skeleton support which could improve the mechanical strength, and the thin branch fibers acted as connections props which could increase the surface area to volume ratio and decrease the pore size, indicating a

*Corresponding author: bowen15@tjpu.edu.cn

potential application in water separation [28]. Obviously, due to its excellent mechanical properties providing by thick fibers and high specific surface area providing by thin fibers, hierarchically structured materials showed excellent properties compared with normal micro or nano structure materials.

In this study, a hierarchically Ag/PA6 TLNM was fabricated by one-step electrospinning and in situ reduction [19]. SEM, TEM, FT-IR and XPS were used to investigate the morphologies and structures of the membranes. Besides, mechanical properties, pore size distribution, hydrophilicity and antibacterial properties against *E. coli* and *S. aureus* of the membrane were studied.

Experimental

Material

Nylon 6 granules (molecular weight 16000, Yubu, Japan), Formic acid (HCOOH, 98 %, Yingda, China), Tetrabutyl-ammonium Chloride (TBAC, Guangfu, China), Silver nitrate ($AgNO_3$, Yingda, China). All solvents and reagents were of analytical grade and used without purification. *E. coli* and *S. aureus* were prepared by Clean Dying Team of Tianjin Polytechnic University.

Preparation of Nanofiber Membranes

Firstly, PA6/TBAC solution was prepared by mixing 14 wt% PA6 and certain amount of TBAC with HCOOH and stirring for 10-12 h to form a stable and homogeneous solution. The Ag/PA6/TBAC spinning solution was prepared by adding 3 % $AgNO_3$ into the PA6/TBAC solution and stirring gently for 0.5 h to form a flavescens solution. For comparison, solution without TBAC was also prepared. Ultrasonic dispersion was used to ensure the uniformity of the solution. All of above solutions were used to prepare membranes by electrospinning with applied voltage of 45 kV, distances of 15 cm from the collector to the tip of the syringe and injection rates of 0.1 m*l*/h respectively. The inner diameter of syringe was 0.45 mm. The temperature was kept at 25±2 °C and relative humidity (RH) was 25±2 %. The nanofiber membranes were collected on the surface of a grounded aluminum foil. Then the membranes were washed by distilled water to remove the effect of $AgNO_3$. Membranes formed with PA6 solution, PA6/TBAC solution, PA6/$AgNO_3$ solution and PA6/TBAC/$AgNO_3$ solution were named PA6 NM, PA6 TLNM, Ag/PA6 NM and Ag/PA6 TLNM respectively. The basis weight of as fabricated nanofiber membrane was 5 g/m^2. The schematic illustration for the fabrication of Ag/PA6 TLNM is given in Figure 1.

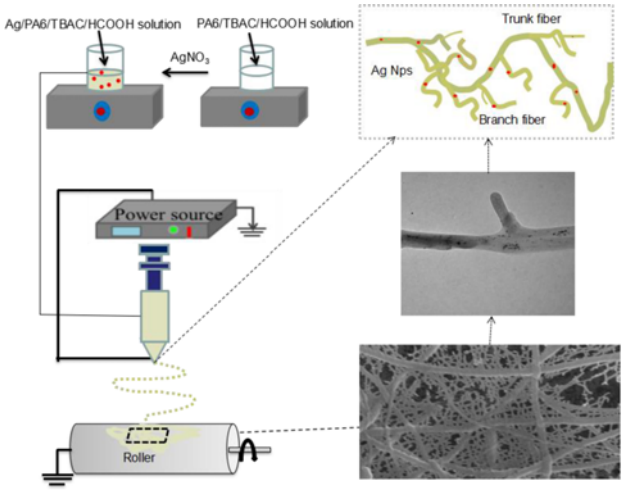

Figure 1. The schematic illustration for the fabrication of Ag/PA6 TLNM.

Characterization

The morphologies of the electrospun membranes were observed using field emission scanning electron microscope (FE-SEM) (S-4800, Hitachi, Japan). The size, shape, and manner of deposition of Ag NPs on the fiber surface were investigated via transmission electron microscopy (TEM) (Hitachi, H-7650, Japan). The structure analysis of as fabricated Ag/PA6 TLNM was conducted using fourier transform infrared spectrometer (FT-IR) (Tensor 37, Bruker, Germany), X-ray photoelectron spectroscopy (XPS) (K-alpha X, Thermo Fisher Co., England). The crystalline phases were identified by X-ray diffraction (XRD) (D8 Discover with GADDS, BRUKER AXS Co., USA) of the samples at 45 kV and 40 mA from 10 ° to 80 ° with an Ni-filtered Cu Kα radiation (λ=0.1542 nm). The mechanical properties of the membranes were measured by monofilament tensile testing machine (YG005E, Wenzhou Fangyuan Instrument Co., Ltd., China), under a speed of 10 mm min^{-1} at room temperature. And five same samples were used to decrease experiment error. The size of the membranes are 50 mm×5 mm. Then membranes with diameter of 4 cm were used to be analyzed by pore size meter (PSM-165, Topas, GmbH, Germany). The water contact angles were analyzed by contact angle tester (JYSP-180, Jinshengxin Instrument Co., Beijing) and the membranes used were 5 cm×5 cm.

Antibacterial Properties

The antibacterial properties of the membranes were evaluated against *E. coli* and *S. aureus* in qualitative agar plate diffusion method. The nanofiber membranes were cut into membranes with diameter of 8 mm and sterilized for 30 min in the clean bench with ultraviolet light (20 W) before they were used. The Luria broth (L B) agar plates containing 1.5×10^6 colonies forming units (CFU/m*l*) of bacteria were used for the culture. Then membranes were pasted in the agar media coating with L B agar plate, incubating at 150 rpm at 37 °C for 12 h, and the antibacterial properties were assessed by the radius of inhibition zone.

Results and Discussion

Morphology of Tree- Like Nanofiber Membrane

Figure 2 shows that the PA6 nanofibers formed from the solution without TBAC exhibit a common circular structure (Figure 2(a1) and (a2)) while nanofibers formed with TBAC shows branch fibers (Figure 2(a3), (a4) and (a5)) which are composed of trunk fibers and branch fibers. And the content of both TBAC and $AgNO_3$ have effects on the morphologies of nanofibers. When the content of TBAC is 3 %wt, only a few branch fibers appear (Figure 2(a4)). When the content of TBAC is 4 %wt, the branch fibers increase and with 3 %wt $AgNO_3$, the tree-like structure appears (Figure 2(a5)). The formation of such hierarchically tree-like structure may be explained by the adding of TBAC. As an organic branched salt [29], TBAC would increase the electrical conductivity of solution (Table 1) and cause the instability of spinning jet when added in spinning solution. Besides, the adding of $AgNO_3$ could also increase the electrical conductivity of solution, but the effect is feeble. Once the excess charge density is above a certain threshold value, the electric forces would overcome the surface tension and form the splitting of the jet. Meanwhile, TBAC could reduce the forces between the PA6 molecules because of its space steric structure, benefiting for the splitting of the jets [28]. Besides, Figure 2(g) shows that Ag NPs are successfully doped in the nanofibers and exist in the surface of nanofibers and Figure 2(h) indicates that Ag NPs not only exist in the trunk fibers but also in branched fibers. Ag NPs existing in branched fibers would contact with bacteria efficiently due to high specific surface area and thinner fibers contributing to the exposure of more Ag NPs.

Spectroscopic Analysis of Nanofiber Membranes

Figure 3 shows the FT-IR spectroscopy of different nanofiber membranes. Peaks at 691.46 cm^{-1} could be assigned to C-H

Table 1. Effect of TBAC content on the conductivity of PA6/ HCOOH solution

TBAC content (wt%)	0	2	4	6	8
Conductivity ($ms \cdot m^{-1}$)	360	390	476	516	586

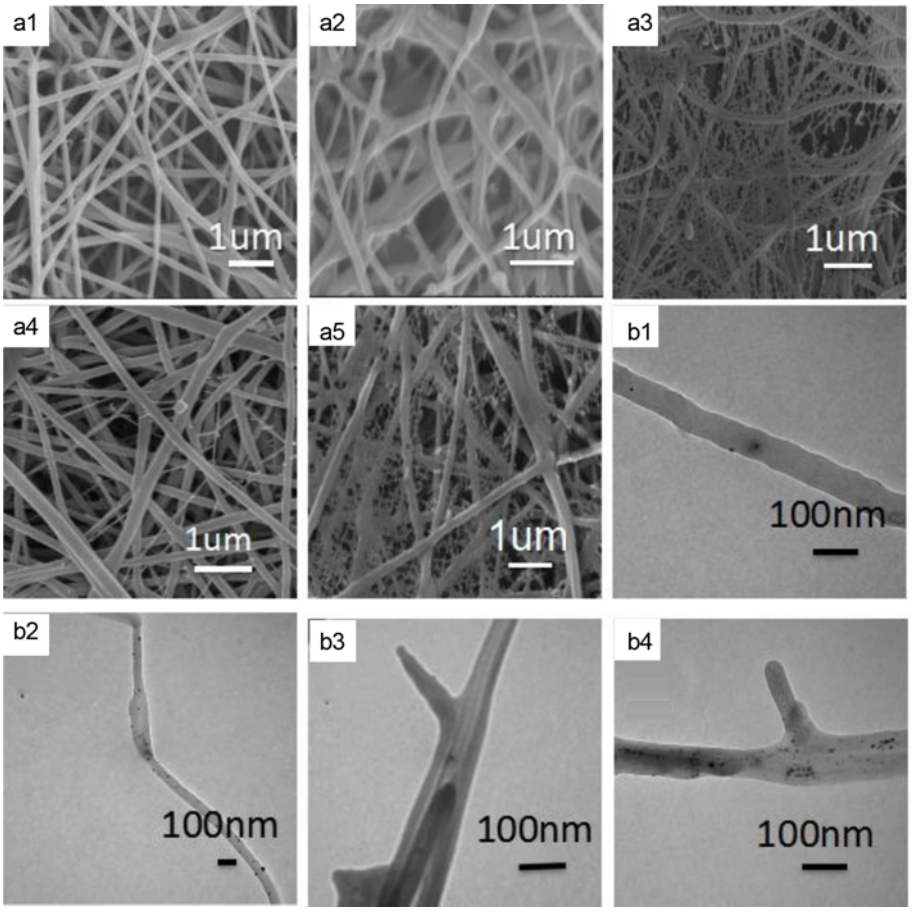

Figure 2. SEM and TEM images of nanofibers; (a1) PA6 NM, (a2) 14 % PA6, 3 % $AgNO_3$, (a3) 14 % PA6, 4 % TBAC, (a4) 14 % PA6, 3 % TBAC, 3 % $AgNO_3$, (a5) 14 % PA6, 4 % TBAC, 3 % $AgNO_3$, (b1) PA6 NM, (b2) 14 % PA6, 3 % $AgNO_3$, (b3) 14 % PA6, 4 % TBAC, (b4) 14 % PA6, 4 % TBAC, 3 % $AgNO_3$.

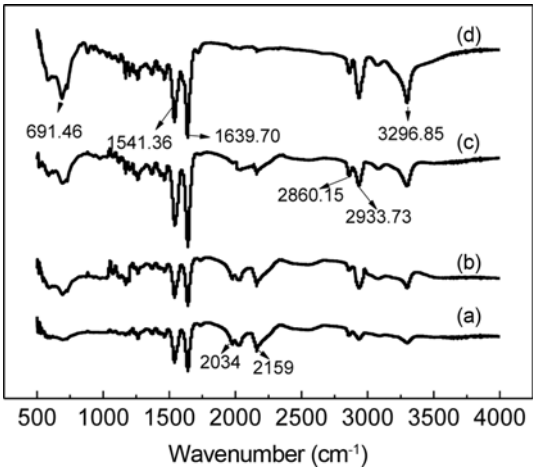

Figure 3. FT-IR spectrums of different nanofiber membranes; (a) PA6 NM, (b) PA6 TLNM, (c) Ag/PA6 NM, and (d) Ag/PA6 TLNM.

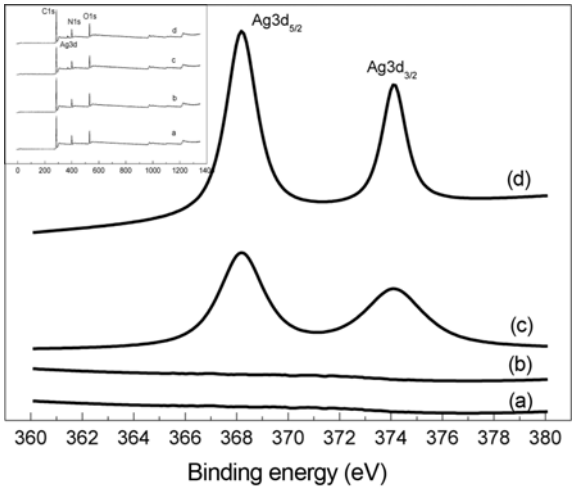

Figure 4. XPS spectrum of different nanofiber membrane; (a) PA6 NM, (b) PA6 TLNM, (c) Ag/PA6 NM, and (d) Ag/PA6 TLNM.

stretching vibration and they appear at all membranes. Peaks at 1541 cm^{-1} and 3296 cm^{-1} are the NH bending vibration and NH stretching vibration and 1639 cm^{-1} is the C=O stretching vibration. Peaks appearing at 2860 cm^{-1} and 2933 cm^{-1} could be attributed to CH_2 stretching vibration. All of above peaks could be attributed to PA6. Peaks at 2034 cm^{-1} and 2159 cm^{-1} are NH_2^+ stretching vibration and the appearance of them could be explained by adding of HCOOH. Due to the existence of HCOOH, polycaprolactammolecular chain is attacked to produce a serious of short chain oligomers, including $CONH_2^+$ and $HCOO^-$ [30] (equation (2)). But NH_2^+ stretching vibration become weak or disappear after adding of $AgNO_3$. With the formation of Ag NPs, they could combine with the NH (equation (3)), resulting in the decrease of the absorption spectra and this interfacial interaction could prevent the oxidation of Ag NPs to some extent [31]. The tree-like structure with high specific surface area would provide more active site to combine with Ag NPs.

$$HCOOH + AgNO_3 \longrightarrow Ag + H_2O + CO_2\uparrow + NO_2\uparrow \quad (1)$$

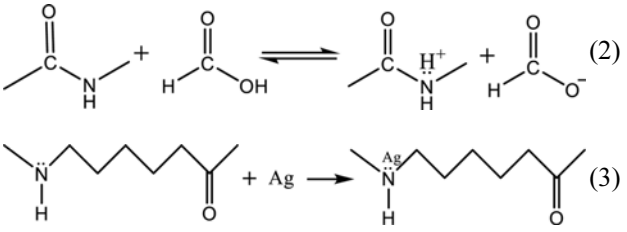

X-ray photoelectron spectrum was used to investigate the formation of Ag NPs. The XPS spectrums of different nanofiber membranes are shown in Figure 4. Firstly, C, N and O elements exist in the membranes without any significantly change in their chemical compositions and Ag/PA6 NM and Ag/PA6 TLNM have a new peak at Ag3d compared with PA6 NM and PA6 TLNM. Further more, in the high-resolution XPS spectrum, two individual peaks at about 368.19 ev and 374.2 ev could be assigned to Ag3d5/2 and Ag3d3/2, which is the characteristic of metal Ag and Ag^+ [32]. XPS analysis had indicated that the content of Ag in Ag/PA6 NM is 0.38 % and Ag/PA6 TLNM is 0.47 %, which further confirmed that more Ag NPs would be exposed on the surface of tree-like nanofibers. Besides, the presence of Ag+ could be explained by the combination of Ag NPs with air.

The XRD patterns of the as fabricated membranes were evaluated in order to study the crystalline phase of PA6 in different environment. Figure 5 shows the XRD pattern of pure PA6 and composites. All of the membranes exhibit a strong diffraction peak at the $2\theta^{o}$ of 22 (2 0 0), which is characteristic of the γ-form, revealing that the pseudo

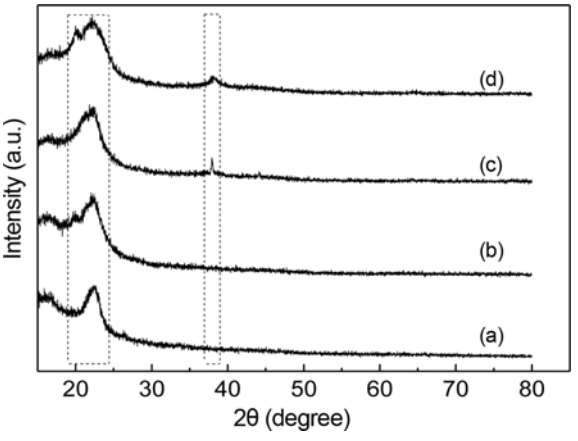

Figure 5. XRD spectrum of different nanofiber membrane; (a) PA6 NM, (b) PA6 TLNM, (c) Ag/PA6 NM, and (d) Ag/PA6 TLNM.

hexagonal γ-form is the dominant phase in the membranes. In addition, in the PA6 TLNM and Ag/PA6 TLNM, the diffraction peaks assigned to the α-form at 20.0 (2 0 0) also appear and the intensity of the peaks is weak. The change in the crystalline behavior of the membranes can be attributed to the adding of TBAC. As an organic branched salt, TBAC would slower the solvent evaporation rate, which allows packing the polymer chain into the thermodynamically more stable α-form [33]. Besides, peaks appearing at $2\theta^{o}$ of 38.2 (1 1 1) are attributed to the loading of Ag NPs [34], which is in good agreement with TEM analysis.

Physical Properties of Nanofiber Membranes

Physical properties of the membrane show a decisive influence on its wide application. Figure 6 shows that the mechanical property of Ag/PA6 TLNM is better compared with Ag/PA6 NM. Tensile stress and strain of the nanofiber membranes increase from 9.9 MPa to 17.1 MPa and 12.5 % to 19.8 % respectively. And the Young's modulus of the membeanes are 0.7698 MPa and 1.3975 MPa respectively. The reason is that the trunk fibers act as support and the branched fibers interact strongly with trunk fibers through the bonding points and the entanglement, resulting in the improvement of the mechanical properties. Besides, Figure 7 also shows that the average pore size of Ag/PA6 TLNM is 0.75 μm while the average pore size of Ag/PA6 NM is 1.75 μm. The decreased pore size of the nanofiber membranes could be ascribed to the compact connections between the dense tree-like branch fibers. Meanwhile, the reduced fiber diameter is contributed to the decrease of pore size [35]. Small pore size and narrow distribution result in a better barrier property towards pollution while ensuring low resistance when used as filters and protection materials, which could be explained by aperture effect [36].

Time-dependent contact angles of the samples were measured to characterize the water wettability and spreading capability of the surfaces (Figure 8). Water could spread on the Ag/PA6 TLNMs and Ag/PA6 NMs in all directions uniformly, endowing membranes excellent hydrophilicity. The contact angles of Ag/PA6 TLNMs significantly decrease within 1second (Figure 8(b1)), whereas there is a slower decrease on the Ag/PA6 NMs (Figure 8(a1)). The phenomenon can be explained by both tree-like structure and adding of TBAC. On one hand, the improved hydrophilicity could be explained by the formation of thinner fibers and the accelerated wicking progress [37]. On the other hand, TBAC could improve the hydrophilicity of the membrane due to its polarity. The hydrophilicity of the membrane depended on synergistic effect of them. Hydrophilic surface could reduce membrane fouling since the hydrophilic surface could repel the fouling adsorption through repulsive hydration force in filtration [38], indicating improved self-clean properties.

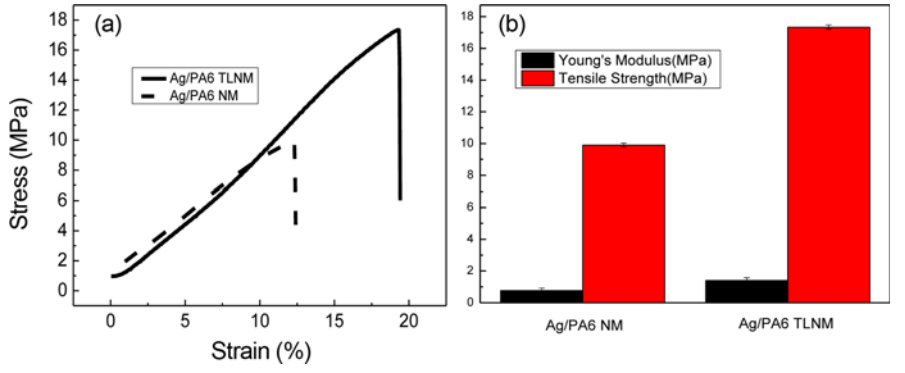

Figure 6. Stress-strain curves of different PA6 nanofiber membranes.

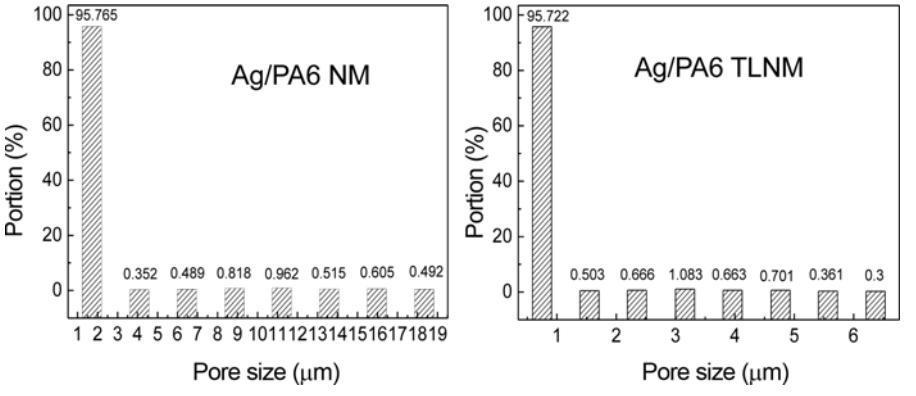

Figure 7. Pore size distribution of different nanofiber membranes.

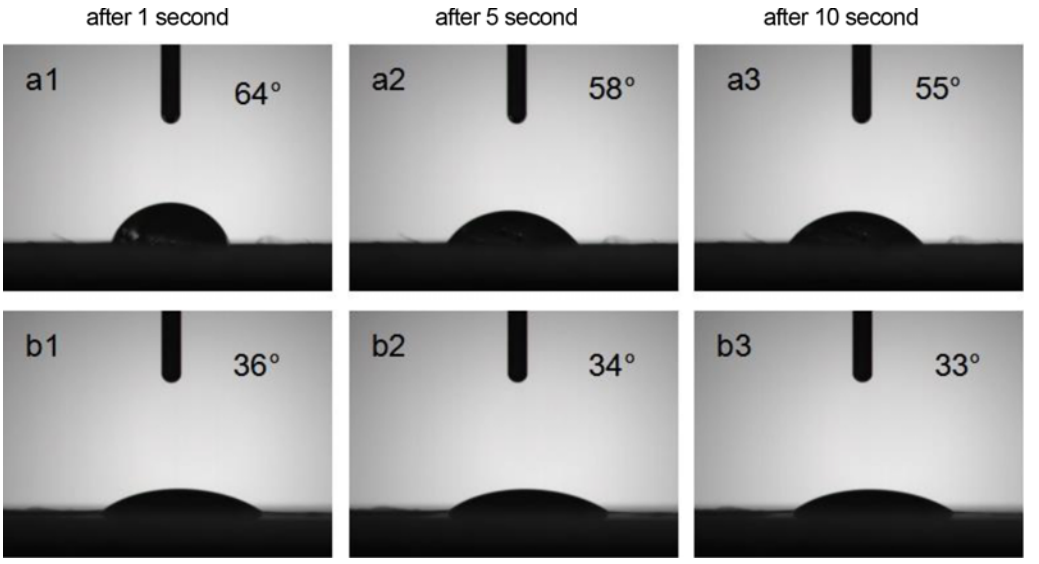

Figure 8. Water contact angles of different nanofiber membranes; (a1, a2, a3) Ag/PA6 NMs, (b1, b2, b3) Ag/PA6 TLNMs.

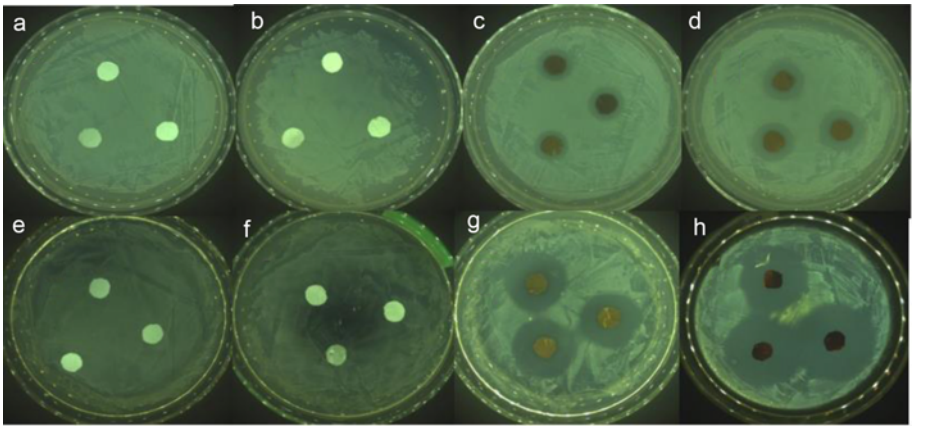

Figure 9. The inhibition zone of different membranes against *E. coli* and *S. aureus* (The upper is *E. coli* and the under is *S. aureus*. (a, e) PA6 NM, (b, f) PA6 TLNM, (c, g) Ag/PA6 NM, and (d, h) Ag/PA6 TLNM).

The Antibacterial Properties of Nanofiber Membranes

The antibacterial properties of the membranes were evaluated against *E. coli* and *S. aureus* by qualitative agar plate diffusion method. Obviously in Figure 9, PA6 NM and PA6 TLNM don't show any antibacterial effect and their radius of inhibition zone are 0 mm (Figure 10). However, Ag/PA6 NM shows remarkable antibacterial properties against *E. coli* and *S. aureus* with decorating of Ag NPs and the radius of inhibition zone are 14.03 mm (*E. coli*) and 25.93 mm (*S. aureus*). And the inhibition zone radius of Ag/PA6 TLNM are 17.34 mm (*E. coli*) and 30.2 mm (*S. aureus*), which is bigger than that of Ag/PA6 NM, indicating that Ag/PA6 TLNM had better antibacterial effect than Ag/PA6 NM. The results could be explained by the high specific surface area of Ag/PA6 TLNM. Ag NPs are not only decorated in the trunk fibers, but also exist in the branch fibers, which could expose more Ag NPs rather than hide them in the

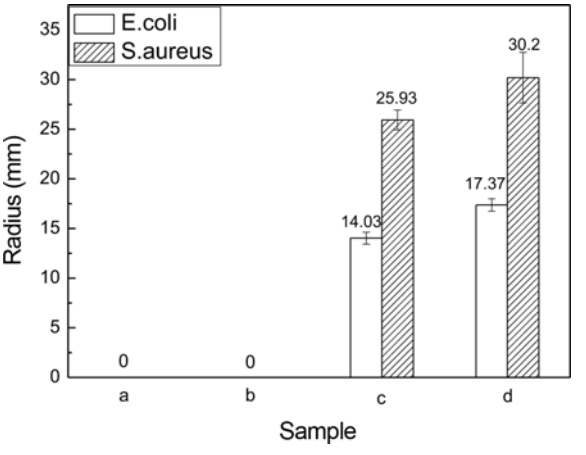

Figure 10. Inhibition zone radius of different nanofiber membranes; (a) PA6 NM, (b) PA6 TLNM, (c) Ag/PA6 NM, and (d) Ag/PA6 TLNM.

inner of nanofibers. The antibacterial properties of nanofiber membranes is mainly determined by the release rate of silver nanoparticles, which is influenced by the content of Ag NPs and the diffusion distance from inside the fiber to the surface [9]. Ag/PA6 TLNM could expose more Ag NPs on the surface of nanofibers and the membrane could gradually release Ag NPs to ambient environment. And then the Ag NPs interact with sulfur-containing proteins and with the phosphorus containing compounds like DNA contained in the cell [9]. They attack the respiratory chain, cell division finally leading to the death of cell. Besides, Ag NPs released Ag^+ in the bacterial cells, which enhances their bactericidal activity [39]. And the slowly release of Ag endows the membrane durable antibacterial property.

Conclusion

A hierarchically Ag/PA6 TLNM was successfully fabricated by a one-step reduction and electrospinning. SEM confirmed that the existence of tree-like structure was due to adding of TBAC. TEM, FT-IR XPS and XRD analyses indicate that Ag NPs are decorated on the surface of tree-like nanofiber steadily and uniformly by one-step reduction. Meanwhile, the appearance of tree-like structure results in better mechanical properties, improved hydrophility, smaller pore size. The antibacterial test shows that membrane with tree-like structure exhibits a superior antimicrobial activity compared with normal PA6 nanofibers membrane. Thus, the Ag/PA6 TLNM would have potential applications in areas such as water purification and separation.

Acknowledgement

The author would like to thank the National Natural Science Foundation of China (51673148, 51102178), the National Key Technology Support Program (2015BAE01B03, 2016YFB0303304), the Science and Technology Plans of Tianjin (15PTSYJC00230, 14TXGCCX00014) and the Fund Project for Transformation of Scientific and Technological Achievements from Jiangsu Province (BA2015182) for their financial support.

References

1. M. J. Hortigüela, L. Yuste, F. Rojo, and I. Aranaz, *Nanomaterials*, **6**, 137 (2016).
2. H. Zhou, J. Li, S. Bao, J. Li, X. Liu, and P. Jin, *Appl. Surf. Sci*., **363**, 532 (2016).
3. J. Y. Park, J. I. Kim, and I. H. Lee, *J. Nanotechnol*., **15**, 5840 (2015).
4. J. S. Kim, E. Kuk, K. N. Yu, J. H. Kim, S. J. Park, and H. J. Li, *Nanomed.-Nanotechnol*., **3**, 95 (2007).
5. D. Wei, W. Sun, W. Qian, Y. Ye, and X. Ma, *Carbohydr. Res.*, **344**, 2375 (2009).
6. O. Akhavan and E. Ghaderi, *Surf. Coat. Technol*., **204**, 3676 (2010).
7. H. J. Jeon, S. C. Yi, and S. G. Oh, *Biomaterials*, **24**, 4921 (2003).
8. P. Rujitanaroj, N. Pimpha, and P. Supaphol, *Polymer*, **49**, 4723 (2008).
9. Z. M. Huang, Y. Z. Zhang, M. Kotaki, and S. Ramakrishna, *Compos. Sci. Technol.*, **63**, 2223 (2003).
10. T. H. Nguyen, K. H. Lee, and B. T. Lee, *Mater. Sci. Eng. C*, **30**, 944 (2010).
11. A. M. Abdelgawad, S. M. Hudson, and O. J. Rojas, *Carbohydr. Polym*., **100**, 166 (2014).
12. S. Wang, J. Bai, C. P. Li, and J. B. Zhang, *Appl. Surf. Sci.*, **261**, 499 (2012).
13. Y. Zhao, Y. Zhou, and X. Wu, *Appl. Surf. Sci*., **258**, 8867 (2012).
14. F. C. Chiu, S. M. Lai, and Y. L. Chen, *Polymer*, **46**, 11600 (2005).
15. H. R. Pant, H. J. Kim, and L. R. Bhatt, *Appl. Surf. Sci*., **285**, 538 (2013).
16. N. Wang, A. Raza, and Y. Si, *J. Colloid. Interface Sci*., **398**, 240 (2013).
17. L. Zhang, J. Luo, and T. J. Menkhaus, *J. Membr. Sci*., **369**, 499 (2011).
18. L. Francis, F. Giunco, A. Balakrishnan, and E. Marsano, *Curr. Appl. Phys*., **10**, 1005 (2010).
19. Q. Shi, N. Vitchuli, J. Nowak, and J. Noar, *J. Mater. Chem.*, **2128**, 10330 (2011).
20. J. Bai, Y. Li, S. Yang, J. Du, S. Wang, and J. Zheng, *Solid State Commun.*, **141**, 292 (2007).
21. K. H. Hong, J. L. Park, I. N. H. Sul, and J. H. Youk, *J. Polym. Sci. Pol. Phys*., **44**, 2468 (2006).
22. H. Bai, Z. Liu, and D. D. Sun, *Phys. Chem. Chem. Phys*., **13**, 6205 (2011).
23. X. Wang, B. Ding, G. Sun, M. Wang, and J. Yu, *Prog. Mat. Sci*., **58**, 1173 (2013).
24. N. Wang, X. Wang, B. Ding, J. Yu, and G. Sun, *J. Mater. Chem*., **22**, 1445 (2012).
25. X. Wang, B. Ding, J. Yu, and M. Wang, *J. Mater. Chem*., **21**, 16231 (2011).
26. H. R. Pant, M. P. Bajgai, K. T. Nam, K. H. Chu, S. J. Park, and H. Y. Kim, *Mater. Lett*., **64**, 2087 (2010).
27. H. R. Pant, M. P. Bajgai, K. T. Nam, Y. A. Seo, D. R. Pandeya, S. T. Hong, and H. Y. Kim, *J. Hazard. Mater*., **185**, 124 (2011).
28. Z. Li, Y. Xu, L. Fan, W. Kang, and B. Cheng, *Mater. Des.*, **92**, 95 (2016).
29. H. Jadhav, E. Taarning, and C. M. Pedersen, *Tetrahedron Lett*., **53**, 983 (2012).
30. J. R. Schaefgen and C. F. Trivisonno, *J. Am. Chem. Soc*., **73**, 4580 (1951).
31. B. Pant, H. R. Pant, D. R. Pandeya, and G. Panthi, *Colloid Surf. A-Physicochem. Eng. Asp.*, **395**, 94 (2012).
32. F. Li, W. Kang, and B. Cheng, *Catal. Commun*., **69**, 150

(2015).
33. M. K. Joshi, A. P. Tiwari, B. Maharjan, K. S. Won, H. J. Kim, C. H. Park, and C. S. Kim, *Carbohydr. Polym*., **147**, 104 (2016).
34. B. Maharjan, M. K. Joshi, A. P. Tiwari, C. H. Park, and C. S. Kim, *J. Mech. Behav. Biomed*., **65**, 66 (2016).
35. D. J. Gohlke and J. C. Tanner, *J. Ind. Text.*, **6**, 28 (1976).
36. P. W. Gibson, H. L. Schreuder-Gibson, and D. Rivin, *AIChE J*., **45**, 190 (1999).
37. Y. Dong, C. K. Liu, R. J. Sun, M. Y. Chen, and X. Yang, *J. Text. Res.*, **36**, 11 (2015).
38. Z. Ma, Z. Mao, and C. Gao, *Colloid Surf. B-Biointerfaces*, **60**, 137 (2007).
39. M. Rai, A. Yadav, and A. Gade, *Biotechnol. Adv.*, **27**, 76 (2009).